MICROSTRUCTURE OF SHEAR ZONES IN FONTAINEBLEAU SANDSTONE

Amine El Bied, Jean Sulem, François Martineau

MICROSTRUCTURE OF SHEAR ZONES IN FONTAINEBLEAU SANDSTONE

A. El Bied, CERMES, Ecole Nationale des Ponts et Chaussées / LCPC, France

J. Sulem *, CERMES, Ecole Nationale des Ponts et Chaussées / LCPC, France

F. Martineau, Laboratoire Central des Ponts et Chaussées, Paris, France

published in: International Journal of Rock Mechanics & Mining Sciences 39 (2002) 917–932

*** Corresponding author**.

Postal address : CERMES, Ecole Nationale des Ponts et Chaussées, 6 et 8 avenue Blaise Pascal, Cité Descartes, Champs-sur-Marne, 77455, Marne-La-Vallée, cedex 2, France.

Phone : + 33 1 64 15 35 45, Fax : + 33 1 64 15 35 62, Email : sulem@cermes.enpc.fr

1. Introduction

It is of fundamental importance in geophysics to understand the interplay between phenomena at the micro-scale level, such as deformation and microstructure evolution and rock properties at the macroscopic scale such as porosity, permeability and strength. The subject of the paper is a detailed analysis of the structure of shear bands in granular rocks. Shear band formation is generally seen as the result of strain localisation in inelastic solids. In brittle rocks it corresponds to the coalescence of clusters of damage to form a failure surface. In geotechnical engineering propagation of localised shear deformation zones of finite thickness is controlled by the softening behaviour of the material inside the band. In structural geology where shear bands are sometimes associated with faults, the evolution of the structure of gouge material inside the band when sheared, controls the behaviour of faulted rock mass under seismic loading.

Shear bands which are zones of localised intense damage appear as weaker than the surrounding rock. Depending on the initial porosity of the rock and on the stress level, compaction and strain-hardening or, on the contrary, dilation and strain softening may occur. Transport properties of porous rocks are essentially controlled by the evolution of the structure of the grain geometry and the pore space (volume, connectivity, tortuosity, shape, etc.). In the last decade important experimental and theoretical studies have been made in this area. The comprehensive paper of David et al [1] summarises the large contribution of Wong and coworkers [2-8] for understanding deformation mechanisms and permeability evolution in rocks. They observed that for rock deforming in the cataclastic flow regime (i.e. for high values of the effective mean stress) porosity and permeability decrease with effective mean stress as the rock undergoes a monotonic compaction. This

phenomenon is more pronounced for triaxial tests as compared to hydrostatic tests which indicates that shear stresses enhanced compaction mechanisms. For highly porous rocks deforming in the brittle regime (i.e. at low effective mean stress), it is observed on the contrary that an increase of the rock bulk porosity (shear-induced dilation) is associated with a decrease of the permeability. This counterintuitive result was obtained for different sandstones with porosity larger that 15% [7,8]. These authors explain qualitatively this phenomenon by the fact that if microcracking induces the pore space to dilate, it may increase the tortuosity and decrease the hydraulic radius. To understand how permeability evolves in due course of rock deformation it is thus important to take into account how the geometry of the pore space is modified during the deformation process.

Shear localisation results from the coalescence near the peak stress of clusters of oriented microcracks due to Hertzian fractures initiated at grain contacts. As observed by David et al [1] the high density of cracks in the shear band is comparable with that of samples 'homogeneously' deformed in the cataclastic flow regime. Detailed observation of shear zones may thus give clues to understand the behaviour of rocks at large stress when pore collapse and grain crushing are important.

The structure of the material inside the shear band has been investigated by several authors (e.g. [9, 10]). Local changes in the microstructure of the rock involving grain crushing and porosity changes have an important influence on the permeability of the material and on the behaviour of the zone of localised failure. To understand the mechanisms of grain cracking and porosity changes inside faults, several authors have studied experimentally the shear-behaviour of sands and crushed rocks which simulate the granular materials found inside the faults (gouge). Examples of such studies can been found in Marone and Scholz [11] who sheared thin layers of quartz sands between steel surfaces with triaxial equipment, Biegel et al [12] who sheared crushed layers of Westerly granite between

sliding blocks of the same rock with a direct double shear apparatus, Morrow and Byerlee [13] who sheared several layers of different gouge types between specimens of Westerly granite. These authors have shown that changes in the porous volume are controlled by the sliding rate. Under biaxial loading on a Gosford sandstone at low confining pressure (15 MPa), Ord et al. [14] have observed highly intra-granular cracking in a narrow zone inside the band whereas in a more diffuse region along the band inter-granular slip and rotation occur. Antonellini and coworkers [15] have shown by testing various sandstones under triaxial loading that a dilatant or a contractant behaviour of the band can be observed depending on initial porosity and confining pressure. Low porosity and low confining pressure lead to the formation of dilatant bands with no cataclasis. High porosity and high confining pressure lead to contractant and cataclastic bands, i.e. bands with high fragmentation and grain crushing, the so-called compaction bands. As emphasised by these authors, a fine layer of crushed material and a porosity reduction within a deformation band may provide a natural barrier to fluid flows in hydrocarbon reservoirs and aquifers. Changes in the structure of fault material may also trigger fault sealing. Similar compaction bands have been observed by Olsson [16] for axisymmetric confined tests on Castelgate sandstone. On Vosges sandstone with a porosity of 25%, Bésuelle et al. [17] have made similar observations of dilatant and contractant bands depending on the confining pressure. An interesting phenomenon of patterning is mentioned by these authors for high confining pressures tests. At 50 MPa of confining pressure several shear bands (so-called microscopic bands) with strong porosity are observed. These microscopic bands are surrounded by zones of lower porosity corresponding to a compaction mechanism around the dilating bands. Sequential development of cataclastic bands was obtained on high porosity sandstone (22%) for large diameter samples under 34 MPa of confining pressure by Mair et al. [18]. They observed a number of sets of pale granular strands with

reduced grain size and porosity. On a different experimental setting which allows for shear displacement at the metric scale, Lerat [19] studied the interface behaviour of a Hostun gravel sheared axi-symmetrically in a ring simple shear apparatus. Grain crushing and production of fine particles have been observed at the interface between the gravel and the rotating cylinder. Grain crushing and porosity loss in loose sands compacted at high effective stresses (50 MPa) have been investigated experimentally recently by Chuhan et al [20] for predicting reservoir quality.

In this paper the shear band characteristics in terms of orientation, thickness, porosity and grain-size distribution obtained in triaxial testing on Fontainebleau sandstone are presented and analysed. For this purpose, macroscopic, mesoscopic and microscopic photographs of shear bands have been used. Emphasis is given to the influence of the confining pressure on the formation of dilating or contracting bands. Porosity and grain size changes inside the band are quantitatively evaluated on the basis of image analysis. The extent of the different phenomena such of grain cracking, grain crushing and pore space changes is described.

2. Experimental setting

The model rock chosen for the study is a Fontainebleau sandstone with a porosity of 21%. It is a uniformly graded rock with a grain size of 0.23 mm (Fig. 1). Axi-symmetric strain-controlled triaxial compression tests have been performed at different confining pressures (0, 7, 14, 28 and 42 MPa). The axial displacement is servo-controlled at a fixed rate corresponding to a constant strain rate of 5×10^{-6} sec^{-1} which is slow enough to insure fully drained deformation. The servo-control system allows to control failure and post-peak behaviour. The tests have been stopped close after the maximum axial load (peak strength)

has been reached. Failure along a unique shear band is obtained for confined tests. The zone of localised failure is clearly identified due to the white coloration of the band visible to the naked eye. Similar coloration of the shear zone in sandstone was observed by Ord et al. [14], Bésuelle et al. [17], Mair et al. [18]. This colour change is due to the crushing of quartz grains and allows for a precise evaluation of the thickness and the orientation of the shear band. The interface between the rock specimen and the loading platens of the testing machine is lubricated to avoid friction [21-23]. Cylindrical specimens with a diameter of 40 mm and a height of 60 mm are used. The specimens are instrumented with strain gages for monitoring axial and radial strains. The use of local strain measurements avoid errors due to the compliance of the loading system and the compressibility of the specimen-platen contact. However these measures are reliable only before the state of strain localisation.

The experimental study of shear band characteristics can come up against some difficulties which would make the observation of the localised zone impossible. A major problem to be overcome is to obtain at the end of the test a specimen with a band clearly formed but without any material discontinuity. In Fontainebleau sandstone the cohesion of the rock is essentially due to interlocking of the quartz grains (see Fig. 1). This poorly cemented rock is thus very friable when damaged, leading to important decohesion and sand production during testing. Therefore, the sample is surrounded on its lateral surface with a transparent adhesive tape which prevents the specimen falling apart during deformation. This technique is applied both for dry samples and saturated ones. Furthermore for dry samples, when the adhesive tape is removed, the grains of the sample surface stay glued onto it. It is therefore used as a replica of the surface of the sample when the shear band formed is clearly visible. Such a replica could not be easily obtained for the saturated samples. For a dry sample, microphotographs of the material glued on the tape are shown on Fig.2. Shear-band thickness measurements can be done directly on this support. A print of the shear

band and of all the external surface of the specimen is kept intact on the adhesive tape. Furthermore, this adhesive band does not influence the response of the sample.

3. Macroscopic and mesoscopic observations

3.1. Stress-strain response

In the range of confining pressures used in our tests the behaviour of Fontainebleau sandstone is rather brittle. The tests have been stopped just after the peak of axial load. The corresponding axial strain is around 0.5% for low confining pressure and 1% for higher ones. The overall stress-strain response for dry samples is presented on Fig. 3. For these tests the axial and radial strains at peak strength are shown on Fig. 4. The maximum axial stress is plotted vs the confining pressure (Fig. 5a) for dry and drained tests. This graph shows the pressure-dependent character of the behaviour of Fontainebleau sandstone. The effective yield stress can be fitted with a parabolic Hoek and Brown criterion $\sigma_{axial} = \sigma_{radial} + \sqrt{m\sigma_{radial} + q}$, with $m = 825.7$ MPa^{-1} and $q = 86.5$ MPa. No significant difference is observed between drained tests on saturated samples and tests on dry samples. For each confining pressure, the average effective yield stress is considered and the Mohr circles are plotted on Fig. 5b.

3.2. Orientation of the shear bands

It is commonly observed that the orientation of the band with respect to the lower principal compressive stress decreases when the confining pressure increases [17], [22], [24-29].

This is the case for triaxial compression and extension tests as well as for biaxial tests [22]. In our tests, the orientation of the shear band is measured on the central part of the specimen, as the shear band is often deviated close to the extremities of it (Fig.6). The measured orientation of the shear band with respect to the minor principal stress axis is presented on Table 1.

These results show that the orientation of the shear band decreases when the confinement pressure increases without significant difference between tests on dry samples and drained tests on saturated ones (Fig. 7).

3.3. Thickness of the shear bands

For sand it is commonly observed that the thickness of the shear band is 10 to 20 times the average grain size (e.g. [27], [30-34]). For sandstone, shear band thickness is found to be about 4 to 10 times the grain size [14, 17, 22, 29]. For our tests, shear band thickness is directly evaluated at the mesoscopic scale, on the external surface of the sample observed with a binocular magnifying glass (Fig. 2). The results are summarised on Table 2 and Fig. 8. They show that the thickness of the shear band decreases when the confining pressure increases. Similar observation has been made by Haïed et al. [29] and Bésuelle et al. [17].

4. Microscopic observations

4.1. Linear porosity

Surface porosity is defined as the void ratio of a given surface and the volumetric porosity

as the void ratio of a given volume. It is important to relate the 2D measurements made on a slide under a microscope with the 3D values. Let us consider a spherical grain with a diameter D_{50}, cut by a plane. If the position and the inclination of the plane are changed, the diameter of the slide of the grain (2D-diameter) varies from 0 to D_{50}. We note $\overline{D}_{50}$ the average 2D-diameter of the grain. As shown by Underwood [35] $\overline{D}_{50} = 2/3\ D_{50}$. Furthermore it is shown by this author that the volumetric porosity of a given volume is equal to the average surface porosity on this volume. The volumetric porosity evaluated by the classical way of rock saturation does not take into account the non connected pores while the surface porosity does. If we assume that the closed porosity is negligible, we can consider that the surface and the volumetric porosity are equal.

Surface porosity can be evaluated using image processing software [17, 36]. As emphasised by Passas et al [36], some difficulties arise in using computer-aided image analysis systems. Careful calibration of the system is needed. Results can be largely dependent on the resolution of the input images and on the threshold of grey level to discriminate between solids and voids. In order to overcome these difficulties a simple and reliable technique of evaluation of linear porosity is used here. On a straight line driven on the microphotograph the ratio η_g of the total length of the segments intersecting grains versus the total length of the line is manually evaluated (Fig. 9). The quantity $1-\eta_g$ represents the linear porosity along the given line. The linear porosity of the material is then evaluated as an average value using a squaring grid on the microphotograph (Fig. 10). The interest of this technique is obviously its simplicity and the high precision of the evaluations as we will see in the following. It is however time consuming and tedious, and cannot be used for systematic analysis of a large data base. For such a purpose it can be also useful to use linear porosity analysis in order to calibrate automatic image processing systems. This will be done in further studies.

From a collection of microphotographs of Fontainebleau sandstone with various known porosities (5%, 6%, 21%, 28%) [23, 37-39], the above technique is applied and the corresponding linear porosity is compared with the volumetric one (Table 3). This table shows that these two quantities are equal for a large range of porosity values. This gives confidence to the fact that the linear porosity evaluated as above gives a good approximation of the volumetric one.

4.2. Microscopic photographs

For a set of specimens tested in the laboratory under various confining pressures microphotographs of the shear band zone are made using an electron scanning microscope. In particular, two specimens with a porosity of 21 % have been studied: specimen K73 tested under a confining pressure of 7 MPa and specimen K25 tested under a confining pressure of 28 MPa. After the test, the specimen is put into a vacuum bell-jar and is saturated with epoxy resin. A plane cutting of the specimen allows a clear observation of the shear band inside the rock (Fig. 11). A metallization is performed by pulverising carbon. This operation allows better observations with the electron scanning microscope. Some microphotographs of the shear band zone are presented on Fig. 12-14.

Other microphotographs of two other dry specimens (K31 tested under 28 MPa of confining pressure and K99 tested under 42 MPa) made directly on the replica are presented on Fig. 15-16. These replicas can be observed directly with the electron scanning microscope without the need of any preparation. These pictures show in relief the structure of the band.

They show that the specimen tested under low confining pressure (K73) has a shear zone characterised by grain cracking with no grain crushing. Outside the band the grains are intact or hardly cracked and a clear limit between the two zones is seen. On the other hand

for the specimens tested under high confining pressures (K25, K31 and K99) the shear band is characterised by intense grain crushing and pulverisation. Major changes in the grain size distribution is clearly visible. Very small particles with size of the order of micrometer are produced. The fragments are densely packed, which gives an aspect of flour or white powder visible to the naked eye. Outside the shear band, near the limits of the shear band, the grains are cracked but not crushed. The cracking phenomenon decreases rapidly outside the band.

4.3. Porosity evaluation inside the shear band

Sample tested at low confining pressure:

We consider here as an example, the specimen K73 tested under 7 MPa of confining pressure. The linear porosity inside and outside the shear band is evaluated quantitatively from the observation of the microphotographs. It is obtained that the porosity reaches a maximal value of 31.7 % inside the band and decreases rapidly towards the initial value of 21% outside the band at a distance of 1.05 mm from the centre of the shear band (Fig. 17). This case thus corresponds to dilatant shear banding. We can observe on the microscopic photographs (Fig. 12a,c and 13a,c) three different zones, which correspond respectively to a strongly broken material (zone I with thickness 0.3 mm), a strongly cracked material (zone II with thickness 0.43 mm) and a healthy or slightly cracked material (zone III) outside these two zones (Fig. 17). We can note that the thickness of the shear band as measured with the binocular magnifying glass corresponds to the zone of white coloration of the sample. This thickness is about 1.17 mm and thus includes zones I and II.

Sample tested at high confining pressure:

Similar evaluation is performed on specimen K25 tested under 28 MPa of confining pressure. In this case, the porosity reaches a minimal value of 11% inside the band and a maximal value of 36.4% close to the shear-band boundary, at a distance of 0.45 mm from the centre of the shear band (Fig. 18). The porosity decreases towards the initial value of 21% outside the band at a distance of 1.95 mm from the centre of the shear band (Fig. 19). We can again observe on the microscopic photographs (Fig. 20 and 21) three different zones: Zone I with thickness 0.3 mm of crushed material, zone II with thickness 0.18 mm of broken or strongly cracked grains and zone III outside the two others of healthy or slightly cracked material. We may note that the thickness of the shear band as measured with the binocular magnifying glass is about 0.66 mm and includes zones I and II. The shear band characterised by a white coloration visible to the naked eye shows the following pattern: a compacted zone with high grain crushing and low porosity (values between 2 and 19 %) surrounded by a dilated zone with grain cracking and high porosity (Fig. 20 and 21). This shear band is surrounded by a zone with high porosity and healthy grains. Similar observation of compacting shear bands is made by Mair et al. [18]. However using large diameter samples and going to large strain deformation (up to 11.2%) these authors observe a set of several shear bands formed sequentially. In our case we obtain a unique shear band probably due to the fact that we use smaller diameter samples and that the maximum applied axial strain is about 1%. Note a different pattern of a dilating shear band surrounded by a compacting zone was obtained by Besuelle et al. [17] for a Vosges sandstone at 50 MPa of confining pressure.

4.4. Grain size distribution inside the shear band

The evolution of grain size inside the shear band can be quantified directly from the microphotographs with a high magnification obtained with the electron scanning microscope. The following procedure is used. A window of evaluation is chosen inside the shear band. In the considered window, a set of lines is defined and the size of the segment intersecting a grain is measured. Over a great number of measurements, one can define an average number of particles with a size comprised between a given interval. Note that the particle size measured in two-dimensions $\overline{D}$ is converted assuming spherical shape of the grains into the real size in three-dimensions D according to the rule $D = 3/2\,\overline{D}$ (see section 4.1). For the two samples studied here (K73 with 78 grain size measurements and K25 with 263 grain size measurements) the results are shown on Fig. 22. The ratio of the number of particles with a size in a given interval as compared to the total number of particles is evaluated. This ratio is plotted versus the interval of grain diameter. This figure shows that for both samples, an important number of small particles is obtained. For the specimen tested under 7MPa of confining pressure where grain cracking was mainly observed, these small particles result from weathering of grain boundaries. The average particle size is 64.5 μm. The smallest particle size observed here is about 5μm. 42.5% of the particles have a size smaller than $D_{50}/10$ whereas 55% have a size comprised between $D_{50}/10$ (23μm) and D_{50}. These two numbers reflect on one side the weathering effect (creation of a certain amount of very small particles), and on the other side the fact that most grains are fractured in several parts. For the specimen tested under 28 MPa, the average grain size is 19μm. 74% of the particles have a size smaller than $D_{50}/10$ and 26% have a size comprised between $D_{50}/10$ and D_{50}. These numbers show that the dominant effect is here pulverisation of the grains. The smallest grain size observed is 1μm. Only few grains are simply fractured. All grain size measurements are smaller that D_{50}.

These measurements are further used in order to reconstruct a grain-size distribution curve inside the shear band. This curve is plotted like in the classical grading method in terms of mass percentage of the sample with a size smaller than a given passing size. In order to keep things simple, a strong assumption is made for the shape of the grains which are assumed to be spherical. One can relate then the number of particles with a given size to the volumetric fraction of the material with the considered grain size. Assuming homogeneous mass density of the grains, the volumetric percentage is equal to the mass percentage. On Fig. 23 the grain-size distribution curve of the intact rock obtained by sieving is plotted. On the same graph, the simulated grain-size distribution curves of the material inside the shear-band are plotted for the two samples K73 and K25. This figure clearly shows that for the sample K73 tested under low confining pressure, the curve is practically superimposed on the one of the intact rock, but shows also an important fraction of small particles due to the weathering effect at the surface of the grains which occur in the shear zone. The same value D_{50}=230 μm is obtained for the material inside the band and for the intact rock. For the sample K25 tested at high confining pressure the corresponding grain-size distribution curve is moved to the left as compared to the curve of the healthy rock. For this sample, D_{50}=175 μm inside the band and is thus smaller than D_{50} of the intact rock. This curve shows also the important proportion of fines characterised by the 'tail' of the curve for small grain size values. Another ratio currently used is the uniformity factor $C_u = D_{60} / D_{10}$ for the grain size distribution. This factor is 1.7 for the intact rock, 2.1 for the material inside the band for K73 and 3.2 for the material inside the band for K25. These numbers reflect the fact that a wider range of particle sizes is obtained in the band for high confined tests.

5. Discussion and Conclusions

On the basis of image analysis, the structure of the shear bands formed in triaxial testing on a Fontainebleau sandstone is studied. Tests have been performed on dry samples and on saturated ones in drained conditions. Similar observations have been made for the two types of experiments. This can be explained by the fact that the shear band is of small extent and does not modify the overall transport properties of the rock as the fluid can be drained from the two ends of the sample. The observations can be summarised as follows:

(a) Macroscopic observations

A unique shear band was formed close to the peak strength for all confined tests. The shear band is characterised by a white coloration visible to the naked eye. The orientation with respect to the minor principal axis and the shear band thickness decrease with increasing confining pressure, which shows the pressure-dependence character of the rock.

(b) Evolution of the microstructure for tests at low confining pressure

It is obtained that for specimens tested under relatively low confining pressure (7 MPa), the porosity reaches a maximal value inside the band (31.7 %) and decreases rapidly towards the initial value of 21% outside the band. This is interpreted as dilating shear. The shear zone is characterised by important grain cracking.

(c) Evolution of the microstructure for tests at higher confining pressure

For specimens tested under relatively high confining pressure (28 MPa), in the so-called transitional regime, a different patterning is observed. A compacting zone with intense grain crushing and low porosity (values between 2 and 19 %) is observed in the centre of the band. This zone is surrounded by a dilating one with grain cracking and high porosity (up to 36.4 %). The two central zones correspond to the thickness of the white coloration as observed on the sample (i.e. the shear band). This shear band is surrounded by third

zone with high porosity and healthy grains. In the centre of the band, an important number of particles have a very small size, of the order of a micrometer. In terms of mass (or volume) percentage these particles represent a small fraction. Therefore the grain size distribution curve and the evaluation of the D_{50} is not much affected as compared to those of the intact rock. However the number of these small particles is sufficiently high to form a sort of flour of very low porosity with a characteristic white colour visible to the naked eye.

One application of this study is the influence of shear banding on the flow of fluids and contaminants. Although permeability was not directly measured in our experiments, microstructural observations highlight several features which may significantly affect fluid flow and hydraulic properties in a deformed sample. Under relatively high confining pressure, the centre of the shear band is expected to inhibit fluid migration due to reduced grain size and reduced porosity. It has been observed by Fredrich et al [40] that for the Fontainebleau sandstone, a decrease of effective porosity from 20% to 4% is accompanied by a decrease in permeability of four order of magnitude. A similar observation is made for other sandstones with initial high porosity under hydrostatic and triaxial tests by Zhu and Wong [7]. Actually, the powder inside the band fills the reduced porous space and can be a natural barrier to fluid flows. The zones surrounding the centre of the shear band show a strong dilatancy and might on the contrary allow a high permeability. This induces anisotropy of the rock permeability as the fluid flow can be enhanced in the direction parallel to the shear band and significantly reduced in the direction perpendicular to it. In globally undrained conditions, such changes in the microstructure of the rock allows for local fluid exchanges between compacting zones that expel fluid and dilating ones that absorb it. In a near future results on shear band formation in undrained conditions for granular rock will be presented.

At large scale, similar phenomena can be expected in faulted zones when sheared. In a basin or a reservoir, faults and connected fractures are the natural network for fluid migration. A fault is often seen as a layer of finite thickness filled with a cataclastic rock (gouge material). Changes in the structure of the gouge material, such as grain crushing and porosity reduction, will then affect the global permeability of the reservoir.

Acknowledgments

Part of the research presented in this paper is supported by the Commission of the European Community within the frame of the project DGlab-Corinth (EVR1-CT-2000-40005).

References

[1] David C., Menendez B., Zhu W. and Wong T.F. Mechanical compaction, microstructures and permeability evolution in sandstones. Phys. Chem. Earth (A), 2001, Vol. 26, N°1-2 : 45-51

[2] Wong T-f. Micromechanics of faulting in Westerly granite. Int. J. Rock Mech. Min. Sci. & Geomech. Abstr., 1982, Vol. 19 : 49-64.

[3] Zhang, J., Wong, T.-f. and Davis D.M., Micromechanics of pressure-induced gram crushing in porous rocks, .J Geophys. Res., 1990, 95 : 341-352.

[4] Menendez, B., Zhu, W. and Wong, T.-f. Micromechanics of brittle faulting and cataclastic flow in Berea sandstone, .J. Struct. Geol.,1996, Vol. 18, N° 1 : l-16.

[5] Zhu, W. and Wong, T.-f. Permeability reduction in a dilatant rock: network modeling of damage and tortuosity, Geophys. Res. Lett., 1996, 23 : 3099-3102.

[6] Wong, T.-f., David, C. and Zhu,W. The transition from brittle faulting to cataclastic flow: Mechanical deformation, J. Geophys. Res., 1997, 202 : 3009-3025.

[7] Zhu,W. and Wong, T.-f. The transition from brittle faulting to cataclastic flow: Permeability evolution, J. Geophys. Res, 1997, 102 : 3027-3041.

[8] Zhu, W. and Wong, T.-f. Network modeling of the evolution of permeability and dilatancy in compact rock, J: Geophys. Res, 1999, 104 : 2963-2971.

[9] Aydin A. Small faults formed as deformation bands in sandstone. Pure appl. Geophys., 1978; 116 : 913-930.

[10] Aydin A. and Johnson A. M. Analysis of faulting in porous sandstones. Journal of Structural Geology, 1983; 5, No 1: 19-31.

[11] Marone C. and Scholz C.H. Particle-size distribution and microstructures within simulated fault gouge. Journal of Structural Geology, 1989; 11, No 7: 799-814.

[12] Biegel R. L., Sammis C. G., Dieterich J. H. The frictional properties of a simulated gouge having a fractal particle distribution. Journal of Structural Geology, 1989; 11, No 7 : 827 to 846.

[13] Morrow C. A. and Byerlee J. D. Experimental studies of compaction and dilatancy during frictional sliding on faults containing gouge. Journal of Structural Geology, 1989; 11, No 7 : 815-825.

[14] Ord A., Vardoulakis I., Kajewski R. Shear band formation in Gosford sandstone. Int. J. Rock Mech. Min. Sci. & Geomech. Abstr, 1991; 28, 5 : 397-409.

[15] Antonellini M.A., Aydin A. , Pollard D. Microstructure of deformation bands in porous sandstones at Arches National Park,Utah, Journal of structural geology, 1994; 16 N°7 : 941-959.

[16] Olsson W. Theoretical and experimental investigation of compaction bands in porous rock. Journal of Geophysical Research, 1999; 104, N° B4 : 7219-7228.

[17] Bésuelle P., Desrues J., Raynaud S. Experimental characterisation of the localisation phenomenon inside a Vosges sandstone in a triaxial cell. Int. J. Rock Mech. Min. Sci., 2000; 37, 8 : 1223-1237.

[18] Mair K., Main I., Elphick S. Sequential growth of deformation bands in the laboratory. Journal of structural geology , 2000; 22 : 25-42.

[19] Lerat P. Etude de l'interface sol-structure dans les milieux granulaires à l'aide d'un nouvel appareil de cisaillement annulaire. Thèse de Doctorat de l'Ecole Nationale des Ponts et Chaussées, 1996.

[20] Chuhan F.A., Kjeldstad A., Bjørlykke K., Høeg K. Porosity loss in sand by grain crushing – experimental evidence and relevance to reservoir quality. Marine and Petroleum Geology, 2002, 19 : 39-53.

[21] Labuz J.F. and Bridell J.M. Reducing frictional constraint in compression testing through lubrication. Int. J. Rock Mech. Min. Sci. & Geomech. Abstr., 1999; 30 : 451-455.

[22] Papamichos E., Tronvoll J., Skjaestein A., Unander T.E., Labuz J.F., Vardoulakis I., Sulem J., Constitutive testing of a weak sandstone, Mechanics of Cohesive-Frictional Materials, 2000, 5 : 1-40.

[23] El Bied A. Etude expérimentale et modélisation du comportement des roches granulaires : écrouissage, radoucissement et rupture en mode localisé. Thèse de doctorat de l'Ecole Nationale des Ponts et Chaussées, 2000.

[24] Paterson M.S. Experimental deformation and faulting in Wombeyan marble. Bull. Geol. Soc. Am.,

1958; 69 : 465 – 476.

[25] Evans I. and Pomeroy C.D. The strength, fracture and workability of coal. London, Pergamon Press, 1966; 177.

[26] Han C. Localisation of deformation in sand, Ph.D. Thesis, University of Minnesota, Mineapolis, 1991.

[27] Hammad W. Modélisation non linéaire et étude expérimentale de la localisation dans les sables. Thèse de l'Université J. Fourier de Grenoble, France, 1991.

[28] Tronvoll J. Investigation of cavity failures for sand production prediction, Ph.D. Thesis, University of Trondheim, Norway, 1992.

[29] Haied A. and Kondo D. Strain localization in Fontainebleau sandstone : macroscopic and microscopic investigations. Int. J. Rock Mech & Min. Sci., 1997; 34, No. 3-4, 350.

[30] Roscoe K.H The influence of strains in soil mechanics. Géotechnique, 1970; 16: 129-170.

[31] Scarpelli G. and Wood D.M. Experimental observations of shear band patterns in direct shear tests. Deformation and Failure of Granular Materials, Balkema, 1982; 473 – 484.

[32] Vardoulakis I. and Graf B. Calibration of constitutive models for granular materials using data from biaxial experiments. Géotechnique, 1985; 35, No. 3 : 299 – 317.

[33] Mühlhaus H.B. and Vardoulakis I. The thikness of shear bands in granular materials, Géotechnique, 1987; Vol. 37, No 3 : 271-283.

[34] Vardoulakis I. and Sulem J. Bifurcation analysis in geomechanics, Blackie Academic and Professionnal, 1995.

[35] Underwood E. Quantitative stereology. Reading Massachussetts: Addison-wesley Publishing Company,1970; 274.

[36] Passas N., Butenuth C., De Freitas M.H. A non-volumetric method of measuring the ratio of solids and voids in porous material with a computer aided system. Bulletin de l'Association Internationale de Géologie de l'Ingénieur, Paris, 1996; N°53.

[37] Bourbie T. and Zinszner B. Hydraulics and acoustic properties as a function of porosity in Fontainebleau sandstone. Journal of Geophysical Research, 1985; 90, N°. B13 : 11524-11532.

[38] Zamora M. Etude expérimentale de l'effet de la géométrie de la porosité des roches sur la vitesse des ondes élastiques. Thèse de Doctorat, Université Paris 7, 1990.

[39] Coker D.A., Torquato S., Dunsmuir J. H. Morphology and physical properties of Fontainebleau sandstone via a tomographic Analysis. Journal of Geophysical Research, 1996; 101, N° B8 : 17497-17506.

[40] Fredrich J.T., Greaves K.H., Martin J.W. Pore geometry and transport properties of Fontainebleau sandstone. Int. J. Rock Mech. Min. Sci & Geomech. Abstr., 1993, 30, 7 : 691-697.

CAPTIONS TO FIGURES AND TABLES

Fig. 1 : Microphotograph of a healthy Fontainebleau sandstone.

Fig. 2 : Photographs of shear bands obtained with the binocular magnifying glass. Characteristic white colour on the shear band.

Fig. 3 : Stress-strain response for dry samples

Fig.4 : Axial and radial strains at peak strength for dry samples

Fig. 5 : (a) Yield stress vs confining pressure : (b) Mohr circles

Fig. 6 : Shear band formation : (a) Dry specimen (K73) under 7 MPa of confining pressure; (b): Dry specimen (K99) under 42 MPa of confining pressure.

Fig. 7 : Shear band orientation vs the confining pressure.

Fig. 8 : Thickness of the shear band vs confining pressure.

Fig. 9 : Definition of linear porosity

Fig. 10 : Evaluation of linear porosity : example of squaring grid on a microphotograph.

Fig. 11 : Plane cutting of specimen of sandstone with a shear band after saturation of the rock with epoxy resin.

Fig. 12 : Shear zone observed with an electron scanning microscope from a plane cutting. Dry specimen K73 tested under 7 MPa of confinement pressure. (a) Magnification × 19. (c) Magnification × 38. Saturated

specimen K25 tested under 28 MPa of confinement pressure. (b) Magnification × 15. (d) Magnification × 30.

Fig. 13 : Shear zone observed with an electron scanning microscope from a plane cutting. Dry specimen K73 tested under 7 MPa of confinement pressure. (a) Magnification × 73. (c) Magnification × 147. . Saturated specimen K25 tested under 28 MPa of confinement pressure. (b) Magnification × 76. (d) Magnification × 152.

Fig. 14 : Shear zone observed with an electron scanning microscope from a plane cutting. . Saturated specimen K25 tested under 28 MPa of confinement pressure. (a) Magnification × 305. (b) Magnification × 608.

Fig. 15 : Shear zone observed with an electron scanning microscope from an adhesive tape. Dry specimen K31 tested under 28 MPa of confinement pressure. (a) Magnification × 21. (b) Magnification × 42. (c) Magnification × 63. (d) Magnification × 126.

Fig. 16 : Shear zone observed with an electron scanning microscope from an adhesive tape. Dry specimen K99 tested under 42 MPa of confinement pressure. (a) Magnification × 15. (b) Magnification × 30. (c) Magnification × 63. (d) Magnification × 120. (e,f) Magnification × 240.

Fig. 17 : Sample K73: Porosity distribution as function of the distance from the centre of the shear band.

Fig. 18 : Specimen K25 : Porosity distribution as function of the distance from the heart of the shear band.

Fig. 19 : Specimen K25 : Evaluation of the average porosity (21%) far from the band using a squaring grid on the microphotograph.

Fig. 20 : Microphotograph of a moderately compacting shear band for a specimen under 28 MPa of confining pressure; Zones of crushed, cracked and intact material.

Fig. 21 : Microphotograph of a highly compacting shear band for a specimen under 28 MPa of confining pressure. Zones of crushed, cracked and intact material.

Fig. 22 : Grain size distribution inside the band for samples K73 (7 MPa) and K25 (28 MPa).

Fig. 23 : Grading curves of the intact rock and of the material inside the band for samples K73 and K25

Table 1 : Measured orientation of the shear band.

Table 2: Measured thickness of the shear band.

Table 3: Comparison of evaluated linear porosity with volumetric porosity.

Figure 1

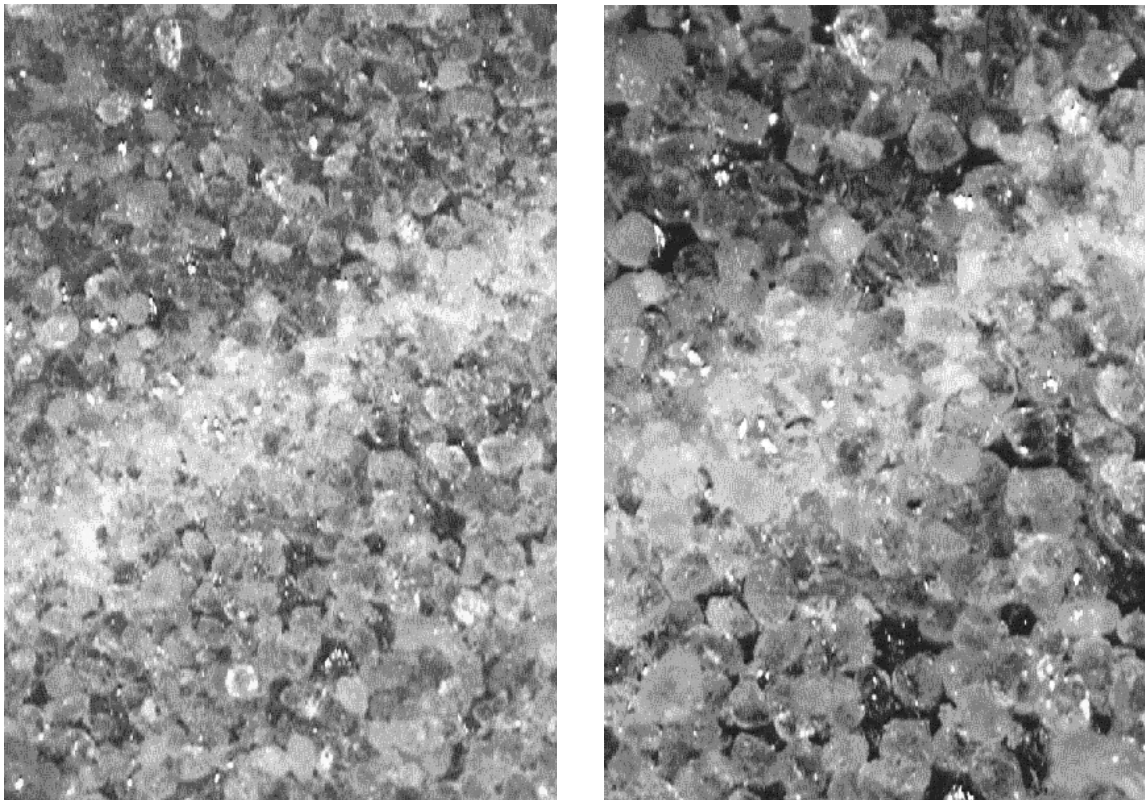

Figure 2

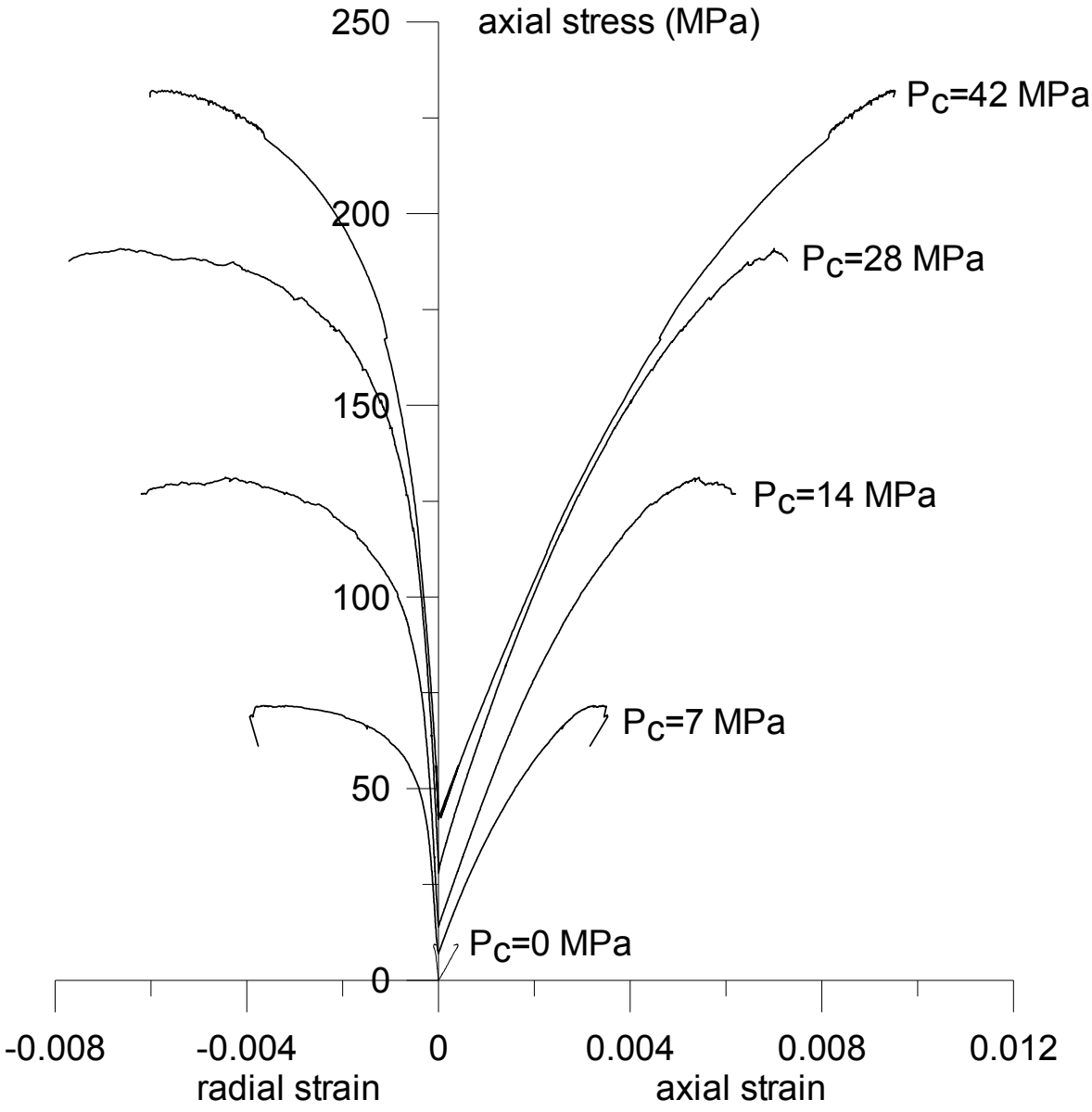
250
axial stress (MPa)
200
150
100
50
0
Pc=42 MPa
Pc=28 MPa
Pc=14 MPa
Pc=7 MPa
Pc=0 MPa
-0.008
-0.004
0
0.004
0.008
0.012
radial strain
axial strain

Figure 3

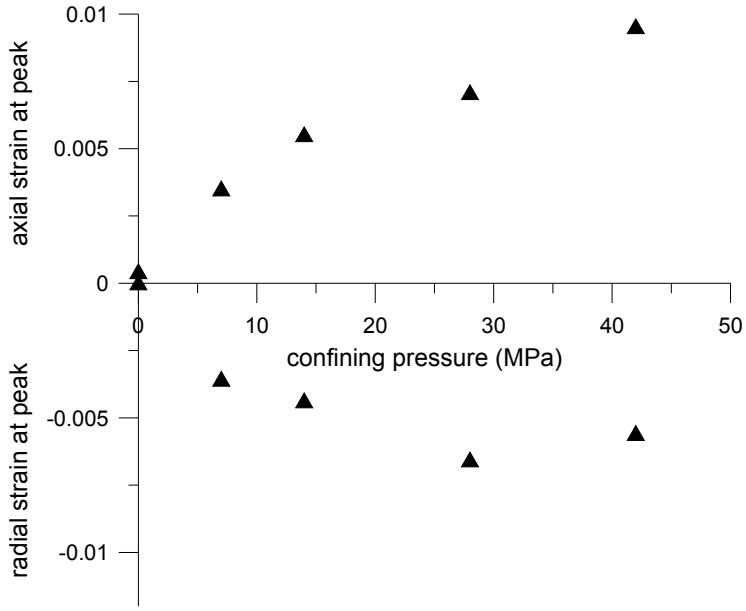
0.01
0.005
0
-0.005
-0.01
axial strain at peak
radial strain at peak
0
10
20
30
40
50
confining pressure (MPa)

Figure 4

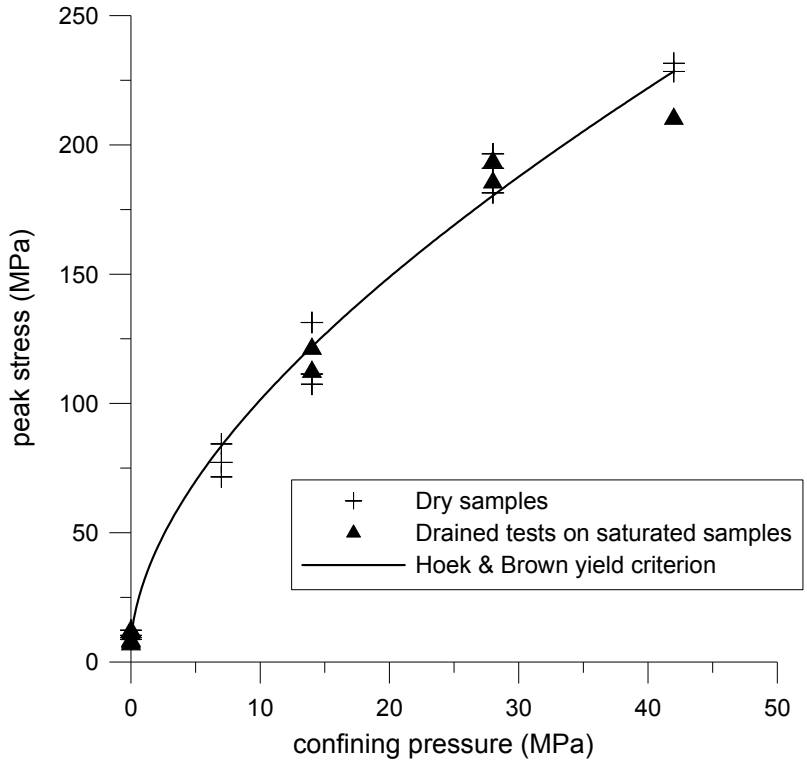
peak stress (MPa)
confining pressure (MPa)
Dry samples
Drained tests on saturated samples
Hoek & Brown yield criterion
(a)

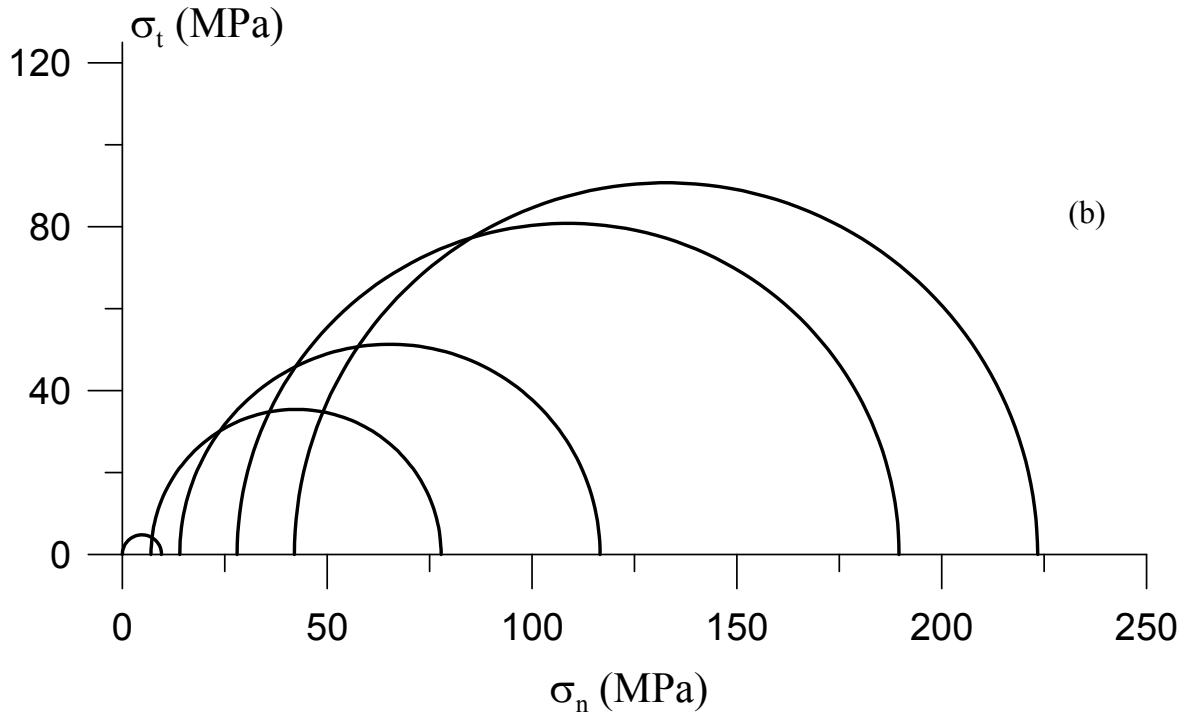
σt (MPa)
σn (MPa)
(b)

Figure 5

(a) (b)

Figure 6

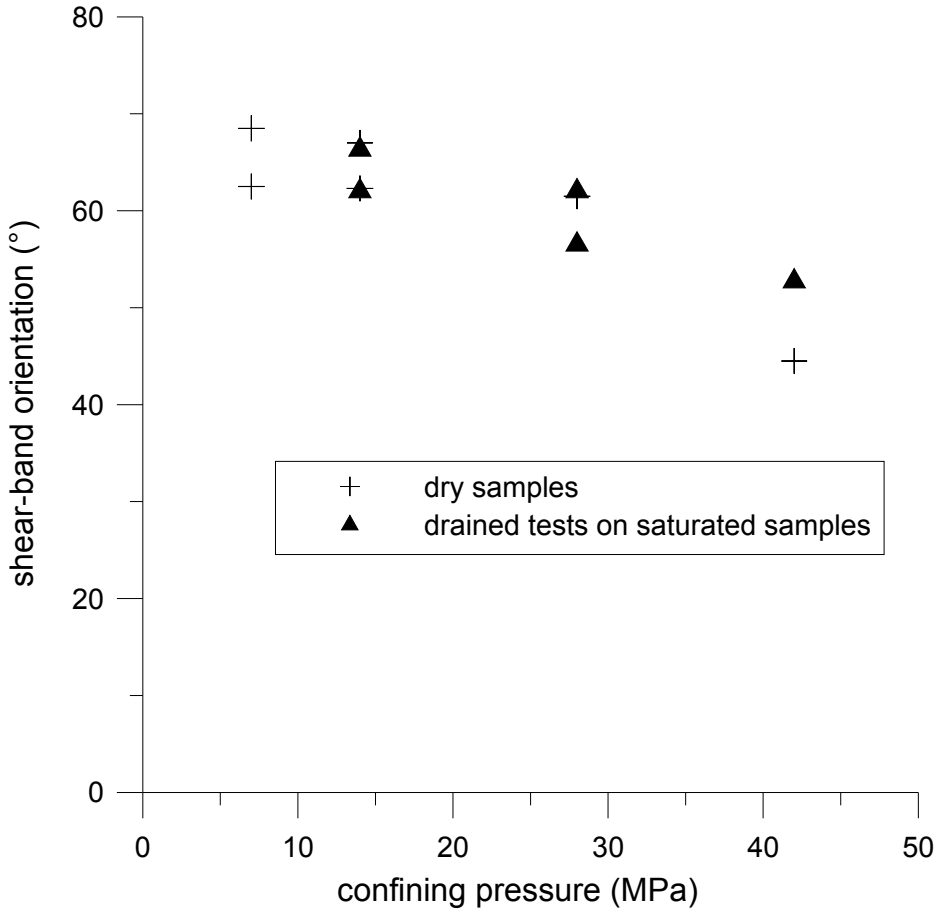
80
60
40
20
0
shear-band orientation (°)
0
10
20
30
40
50
confining pressure (MPa)
dry samples
drained tests on saturated samples

Figure 7

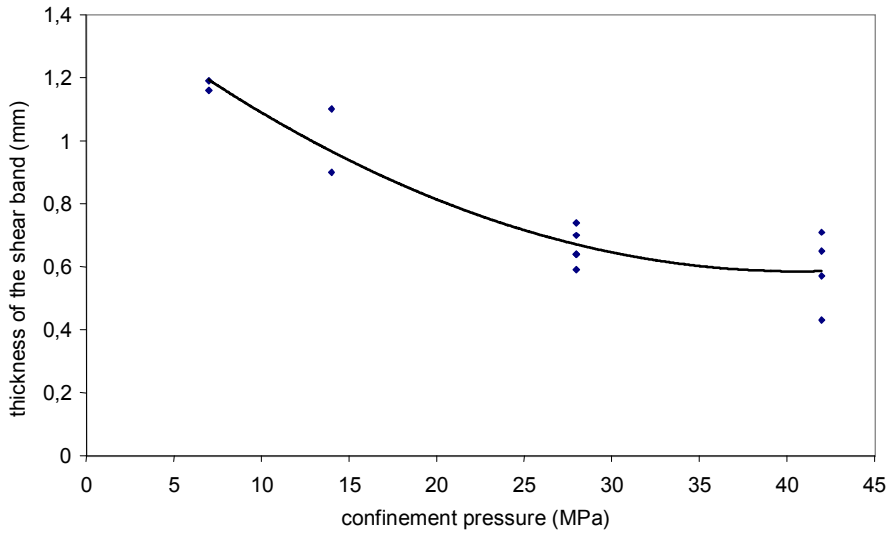
thickness of the shear band (mm)
confinement pressure (MPa)
0
0,2
0,4
0,6
0,8
1
1,2
1,4
0
5
10
15
20
25
30
35
40
45

Figure 8

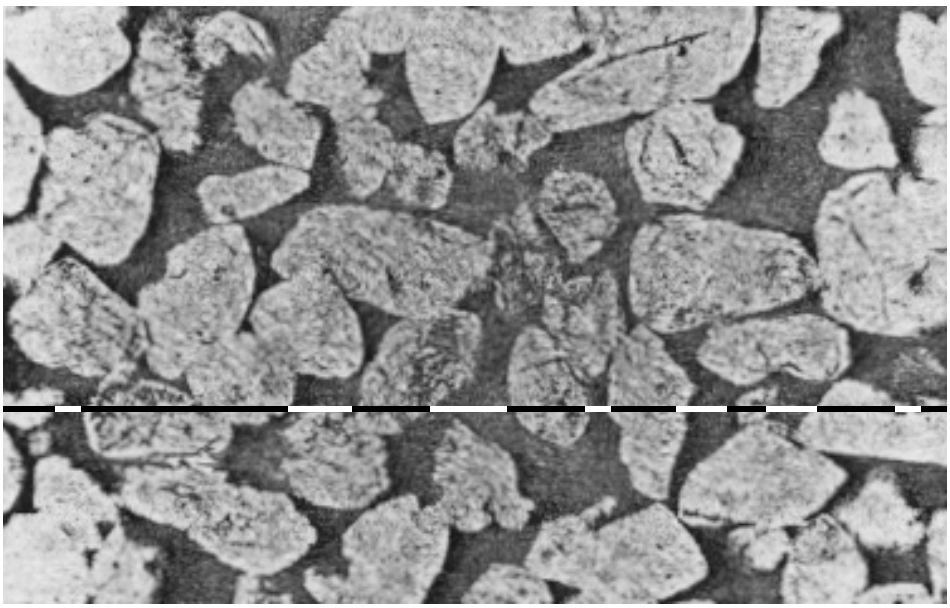

Figure 9

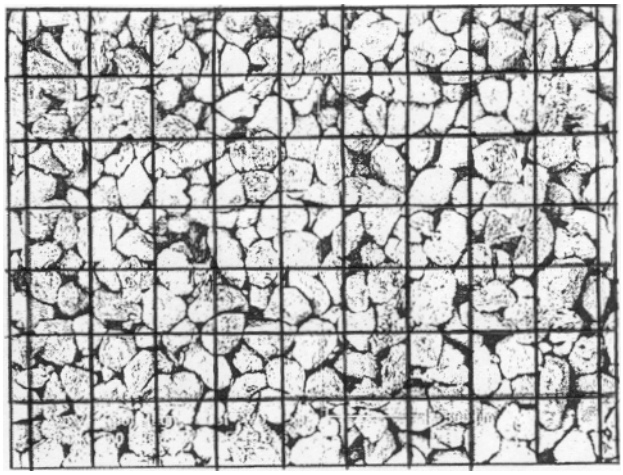

Figure 10

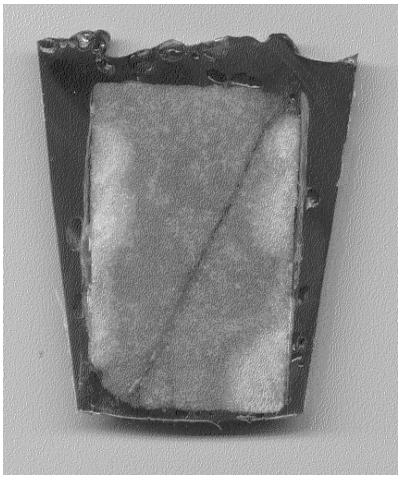

Figure 11

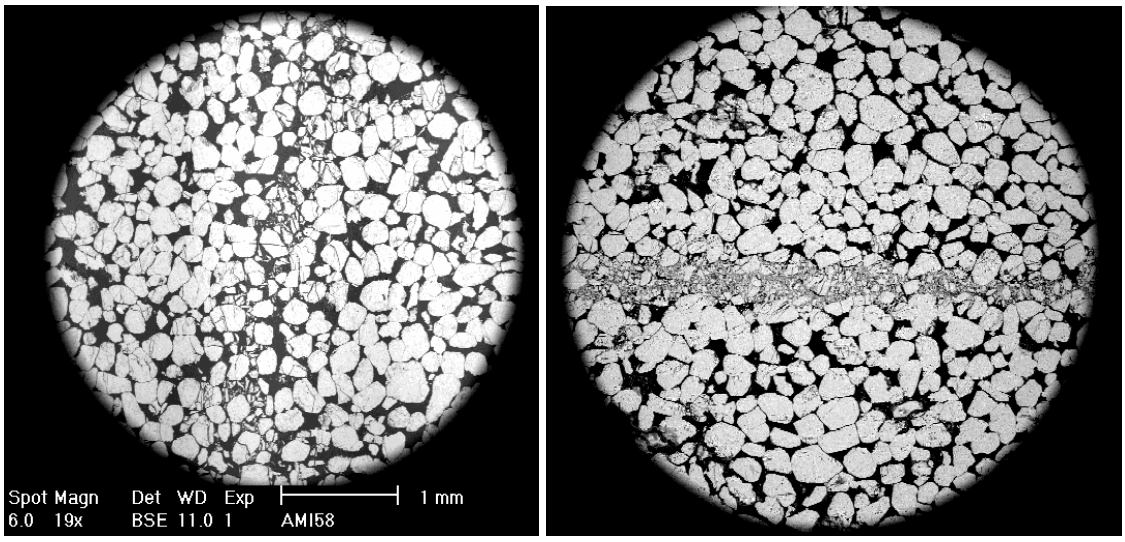

(a) (b)

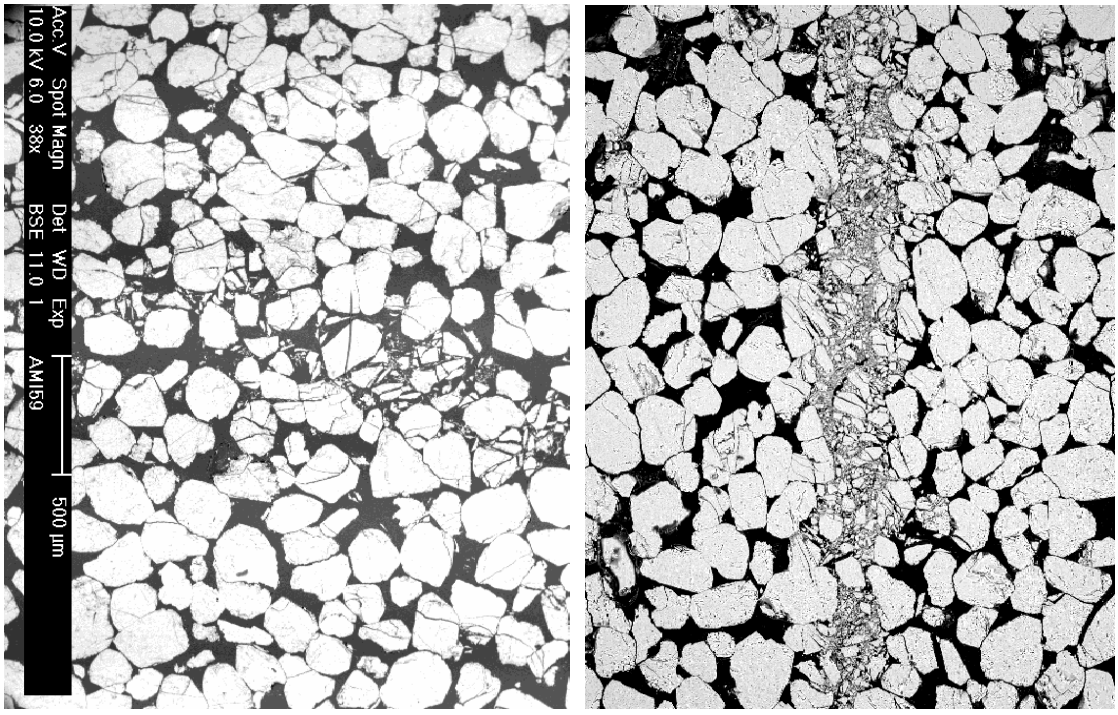

(c) (d)

Figure 12

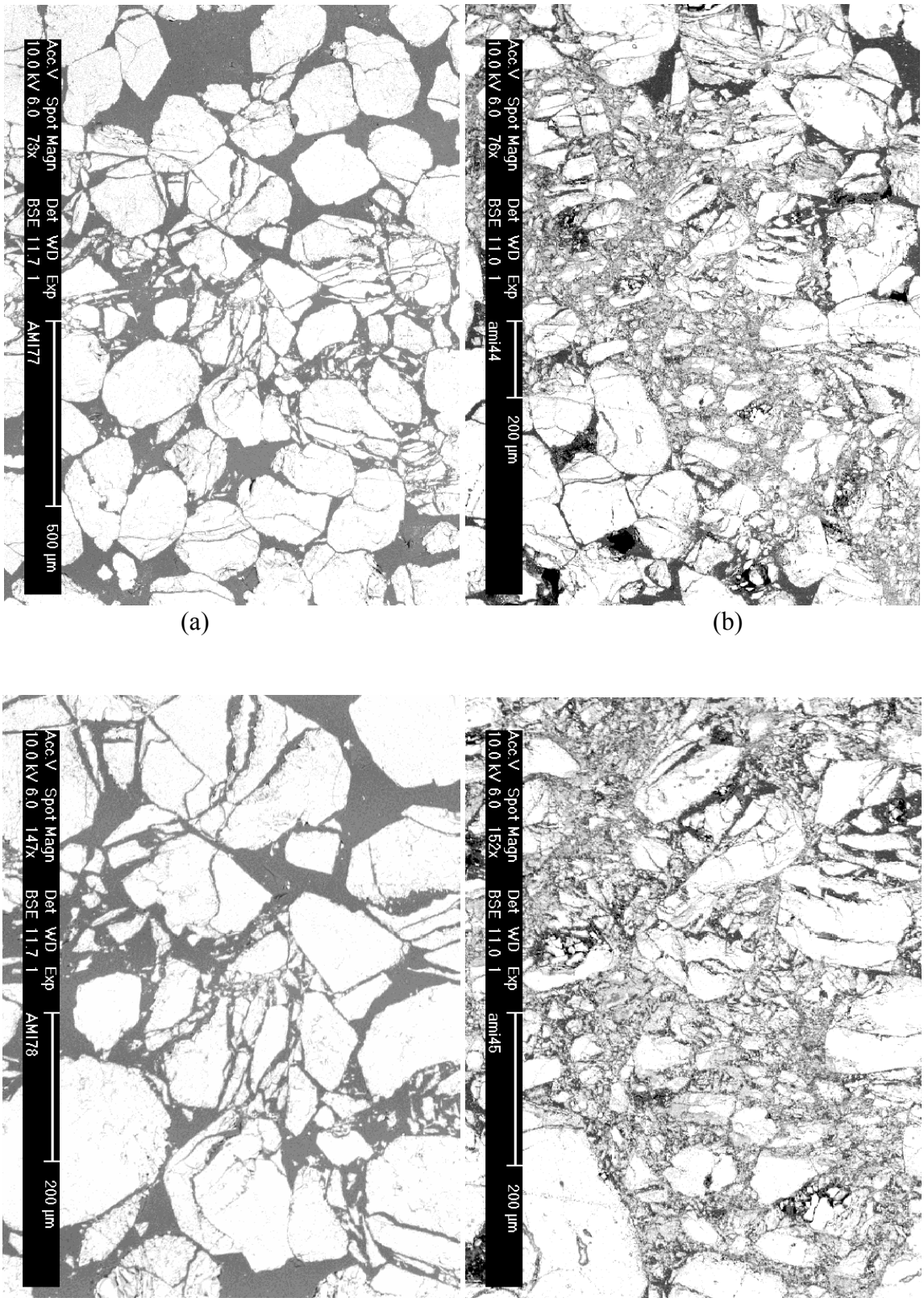

(a) (b)

(c) (d)

Figure 13

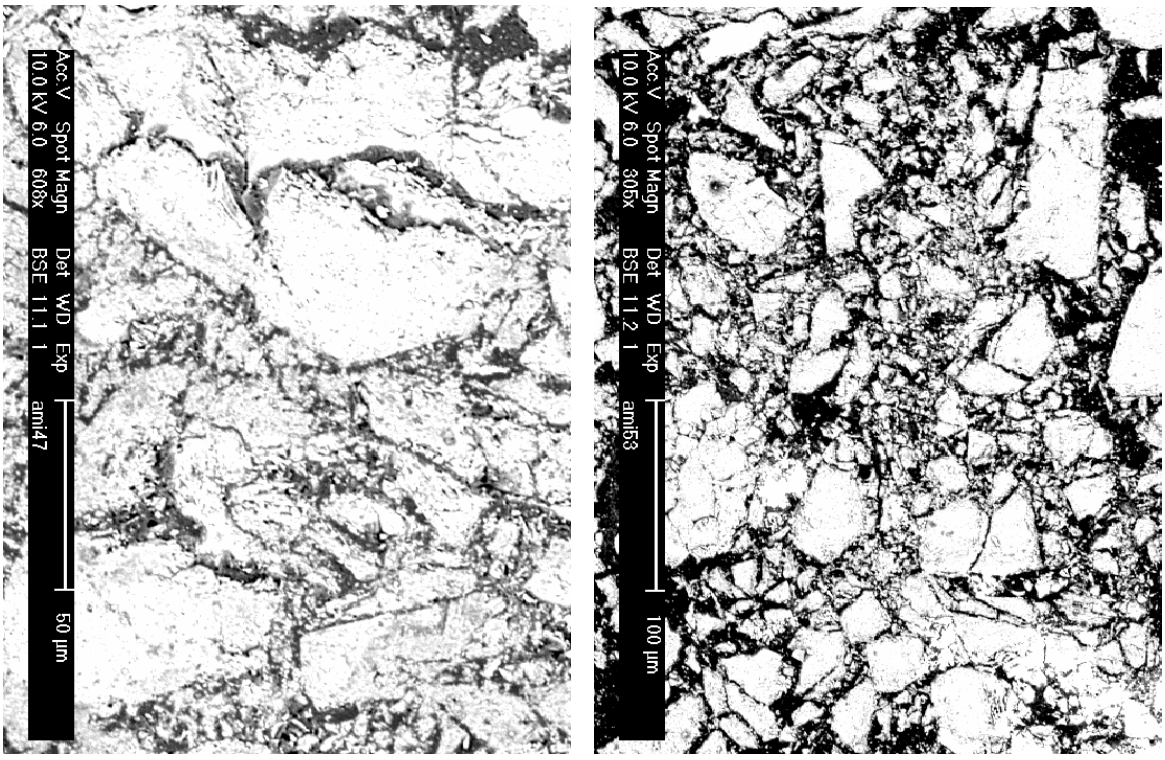
Acc.V Spot Magn Det WD Exp
10.0 kV 6.0 608x BSE 11.1 1
ami47
50 µm
Acc.V Spot Magn Det WD Exp
10.0 kV 6.0 305x BSE 11.2 1
ami53
100 µm

(a) (b)

Figure 14

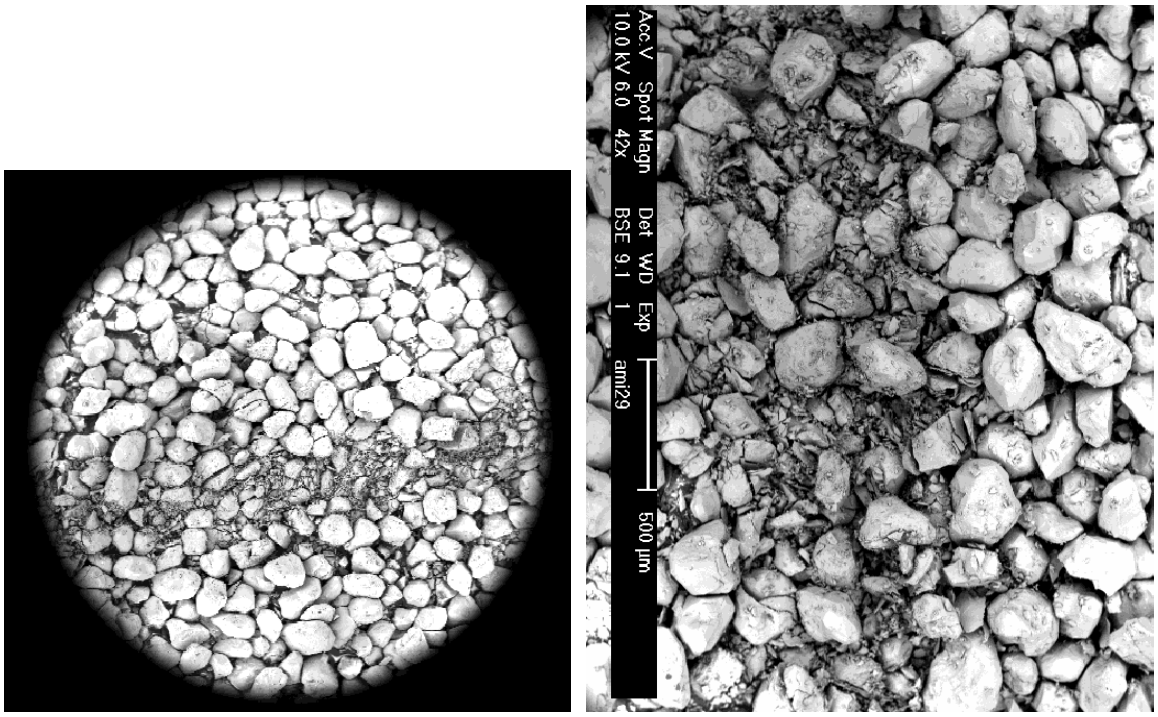

(a)

(b)

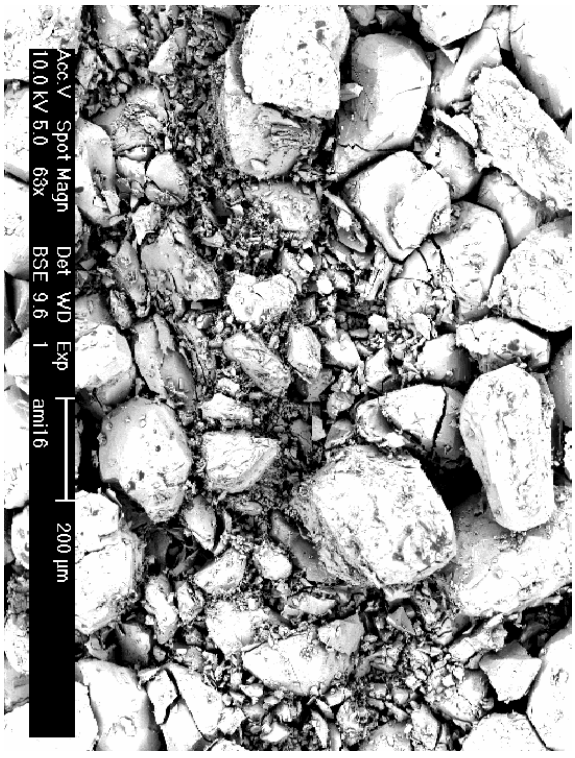

(c)

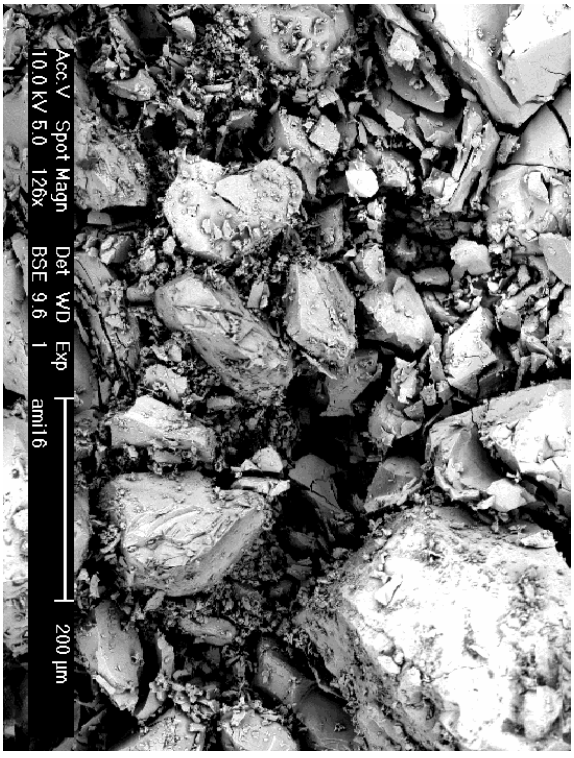

(d)

Figure 15

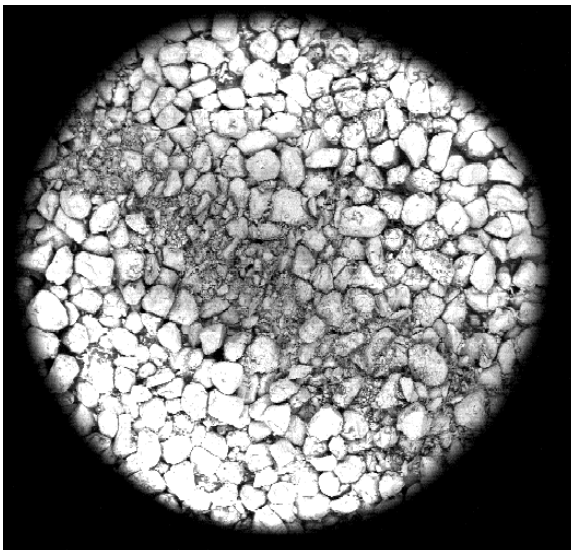

(a)

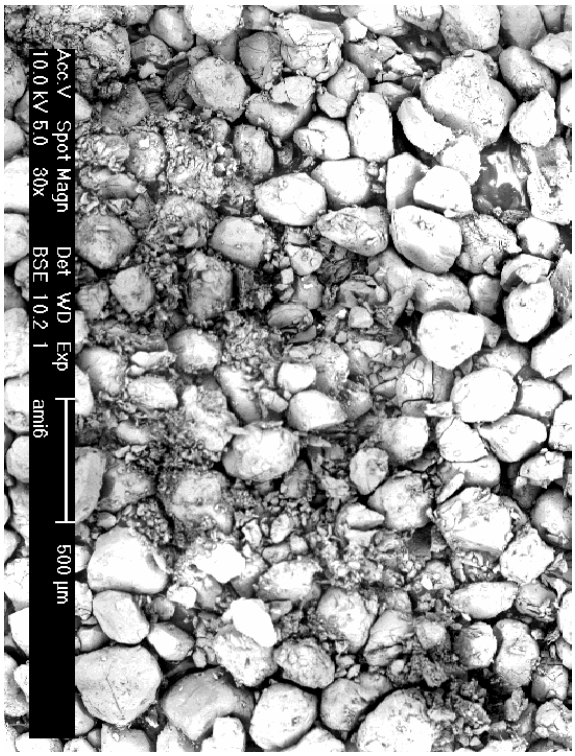

(b)

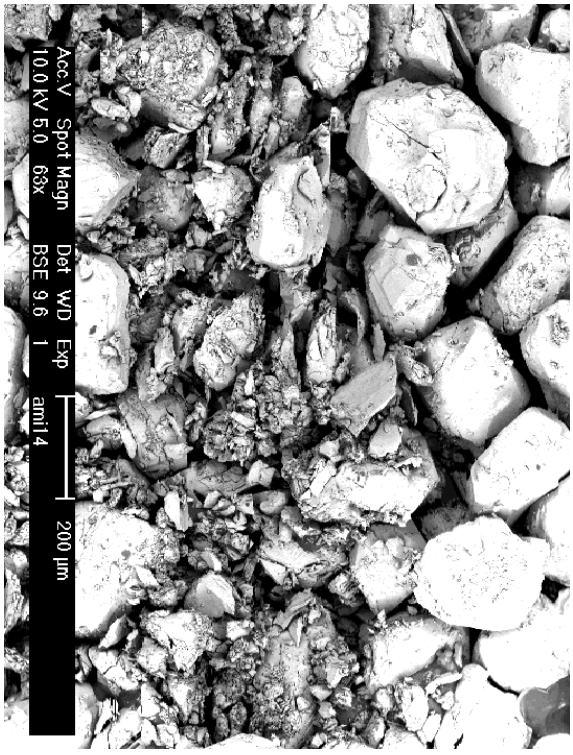

(c)

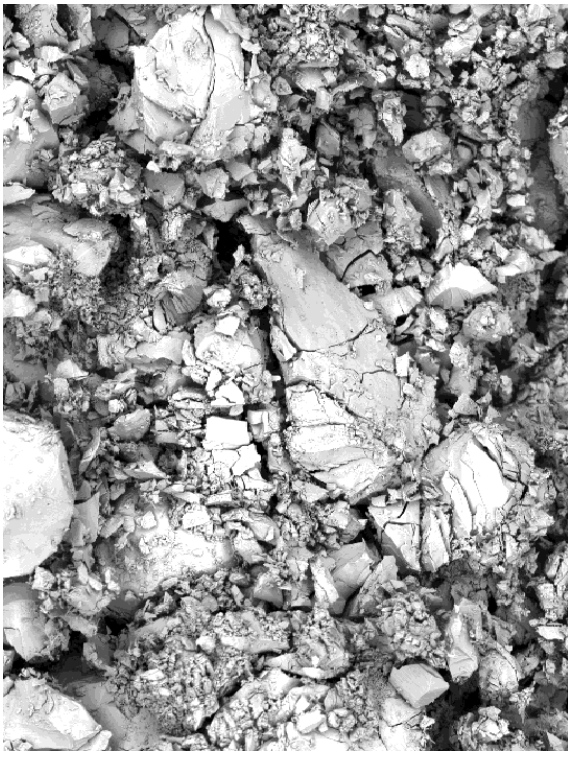

(d)

Figure 16

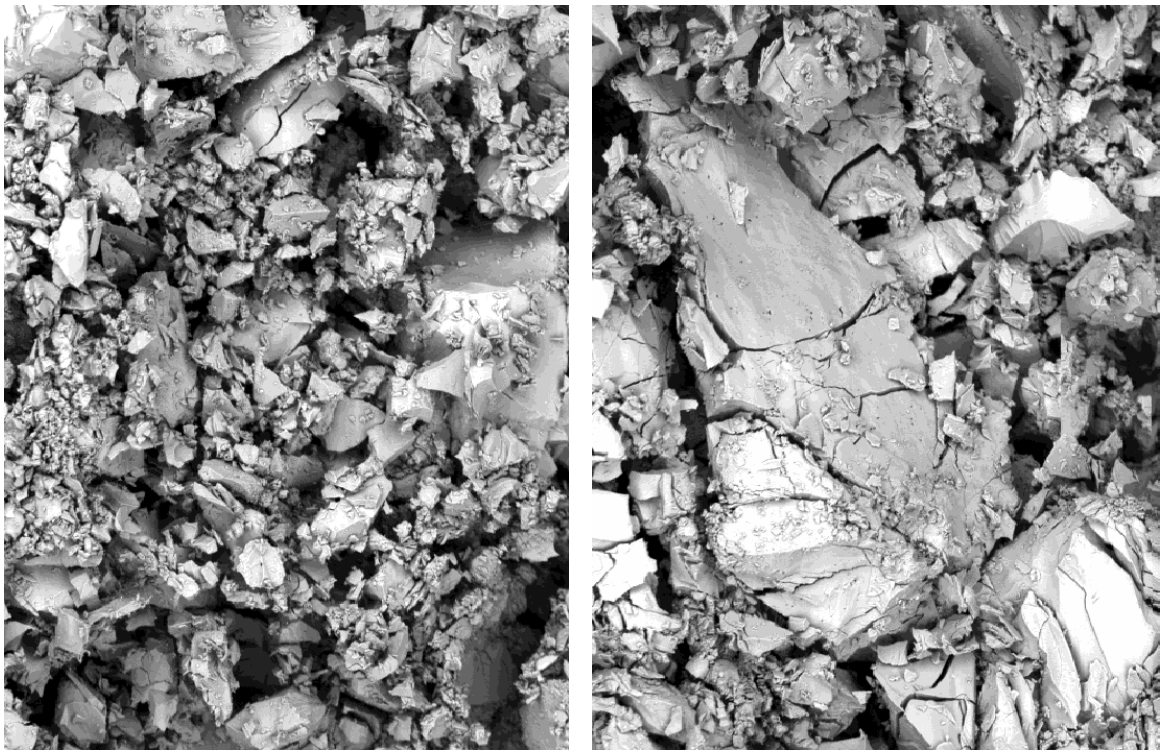

(e) (f)

Figure 16 (continued)

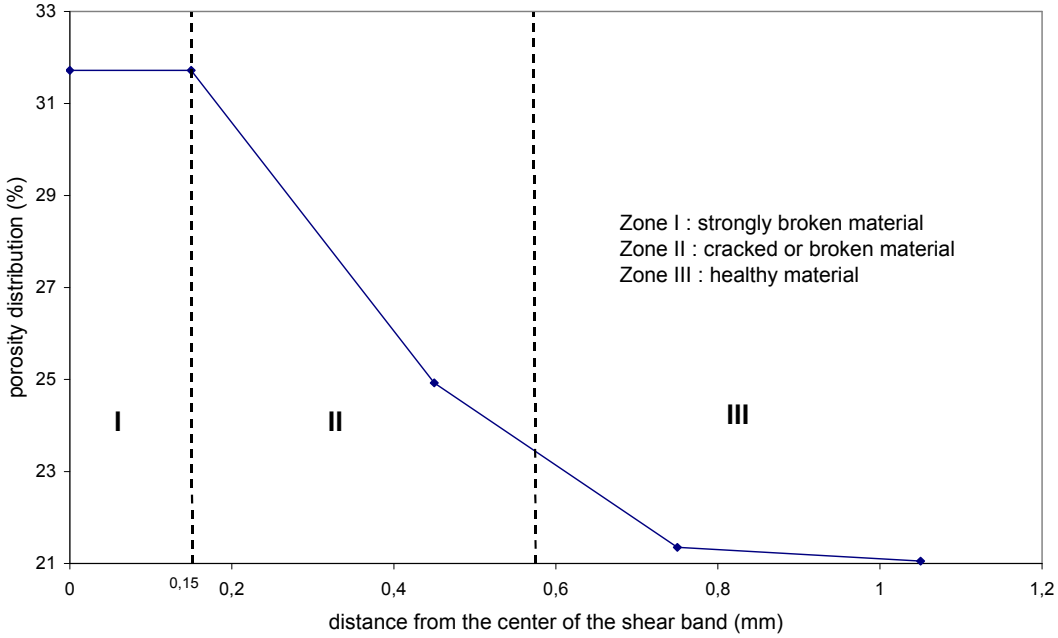
33
31
29
27
25
23
21
porosity distribution (%)
0
0,15
0,2
0,4
0,6
0,8
1
1,2
distance from the center of the shear band (mm)
I
II
III
Zone I : strongly broken material
Zone II : cracked or broken material
Zone III : healthy material

Figure 17

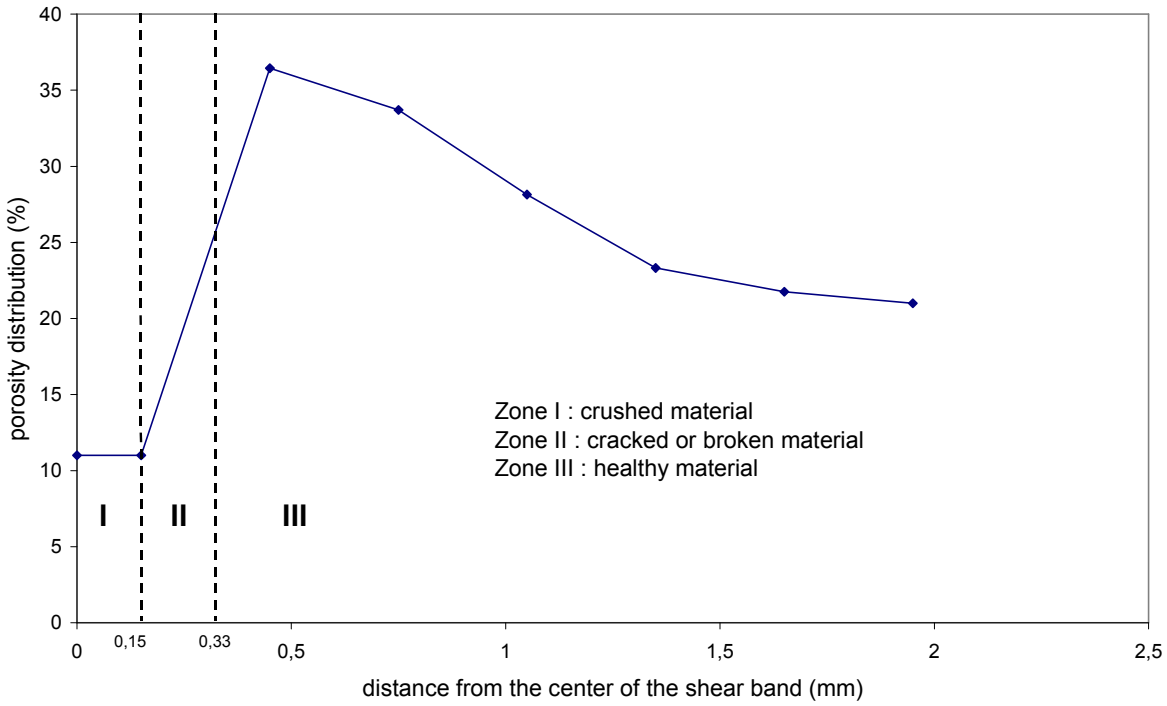
porosity distribution (%)
40
35
30
25
20
15
10
5
0
0
0,15
0,33
0,5
1
1,5
2
2,5
distance from the center of the shear band (mm)
I
II
III
Zone I : crushed material
Zone II : cracked or broken material
Zone III : healthy material

Figure 18

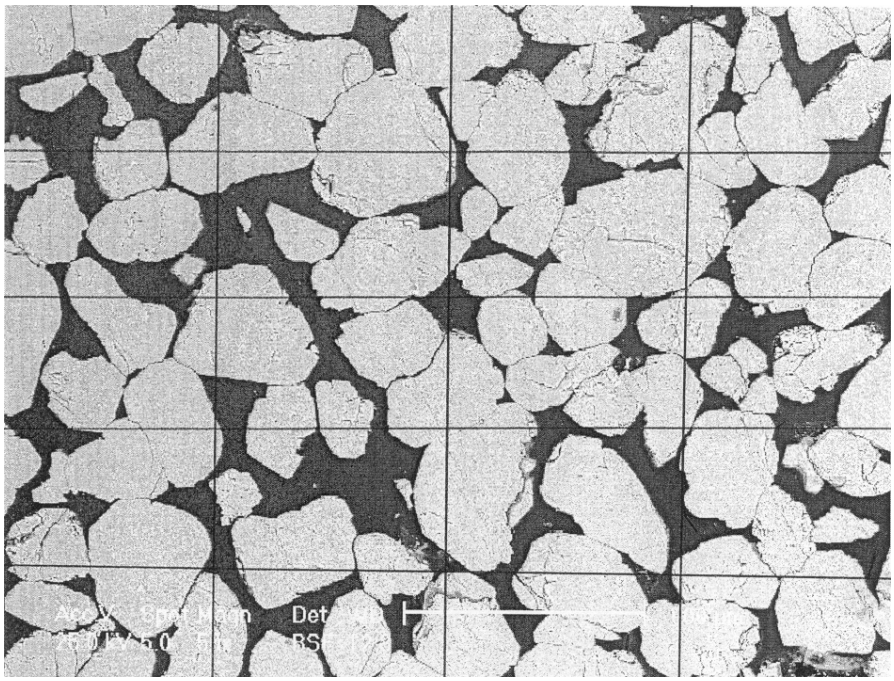

Figure 19

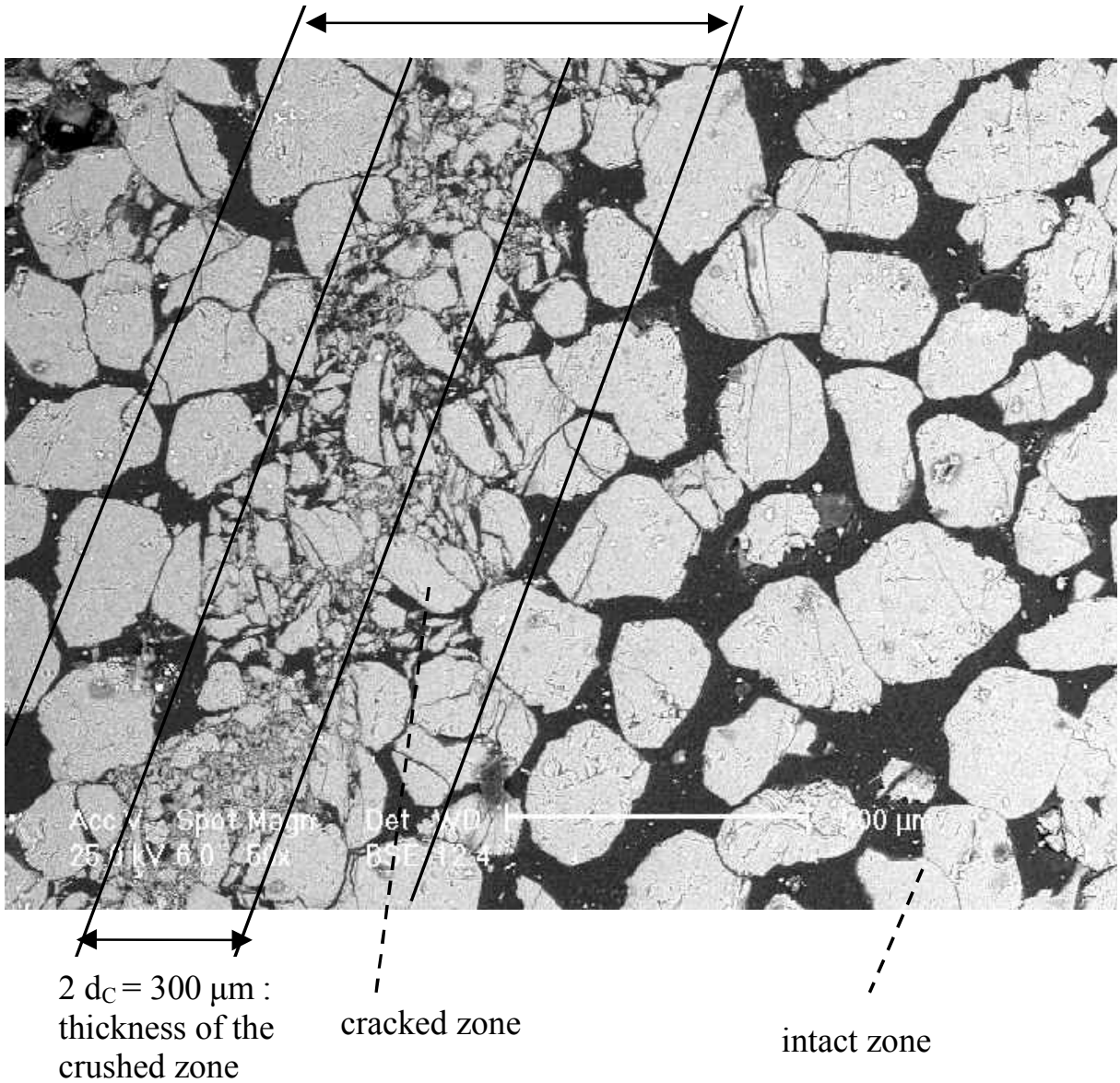
2 d_B = 660 µm : thickness of the shear band as measured with the magnifying glass
2 d_C = 300 µm : thickness of the crushed zone
cracked zone
intact zone

Figure 20

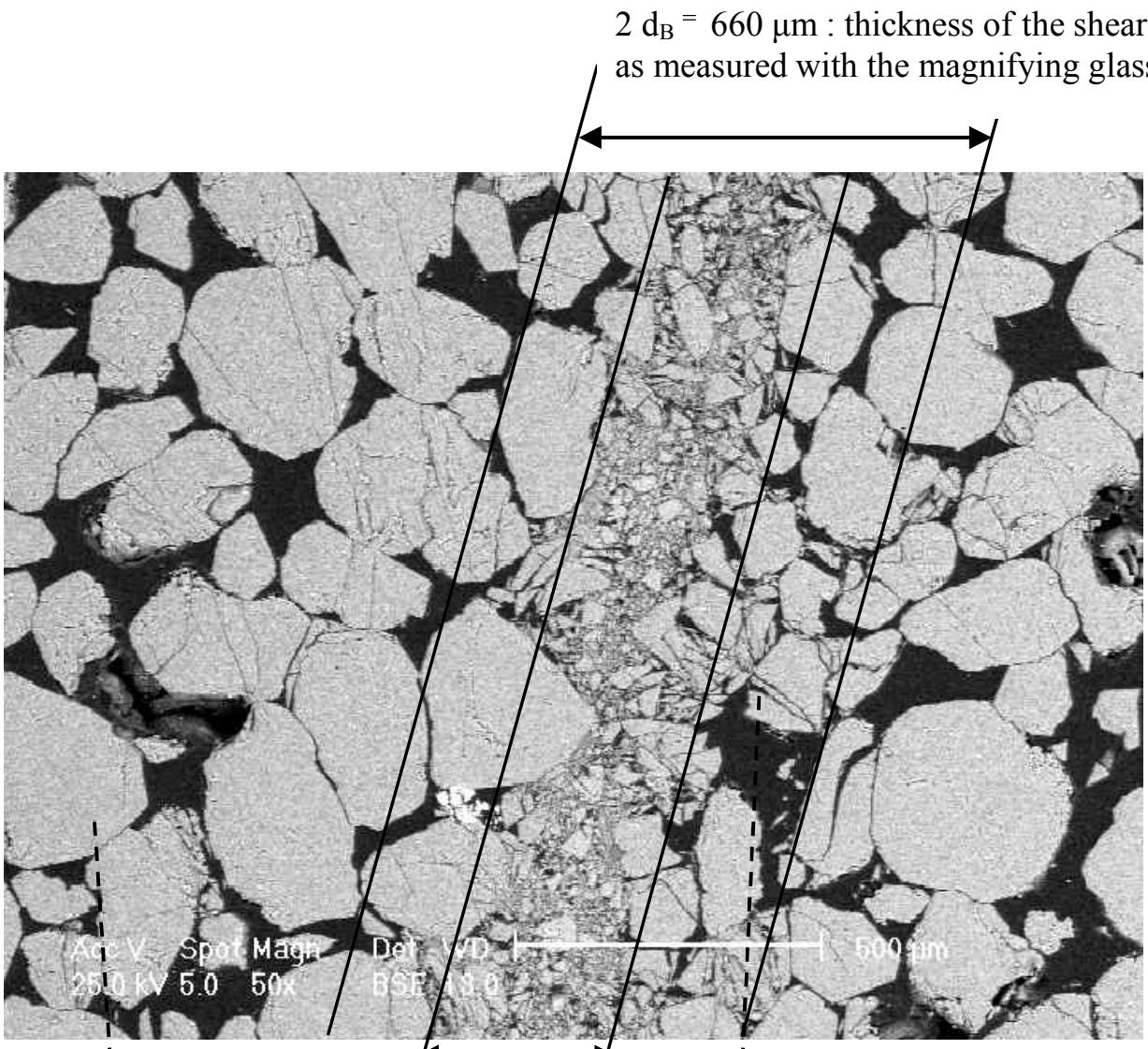
2 d_B = 660 µm : thickness of the shear band as measured with the magnifying glass
Acc.V Spot Magn Det WD
25.0 kV 5.0 50x BSE 13.0
500 µm
intact zone
2 d_C = 300 µm : thickness of the crushed zone
cracked zone

Figure 21

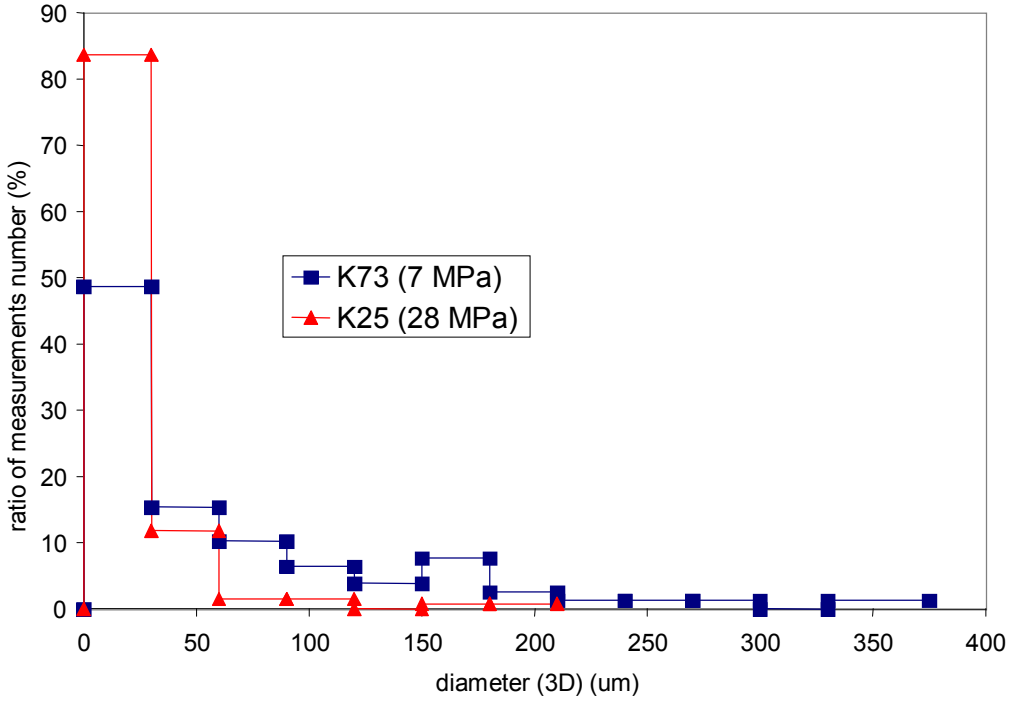
ratio of measurements number (%)
diameter (3D) (um)
K73 (7 MPa)
K25 (28 MPa)
0
10
20
30
40
50
60
70
80
90
0
50
100
150
200
250
300
350
400

Figure 22

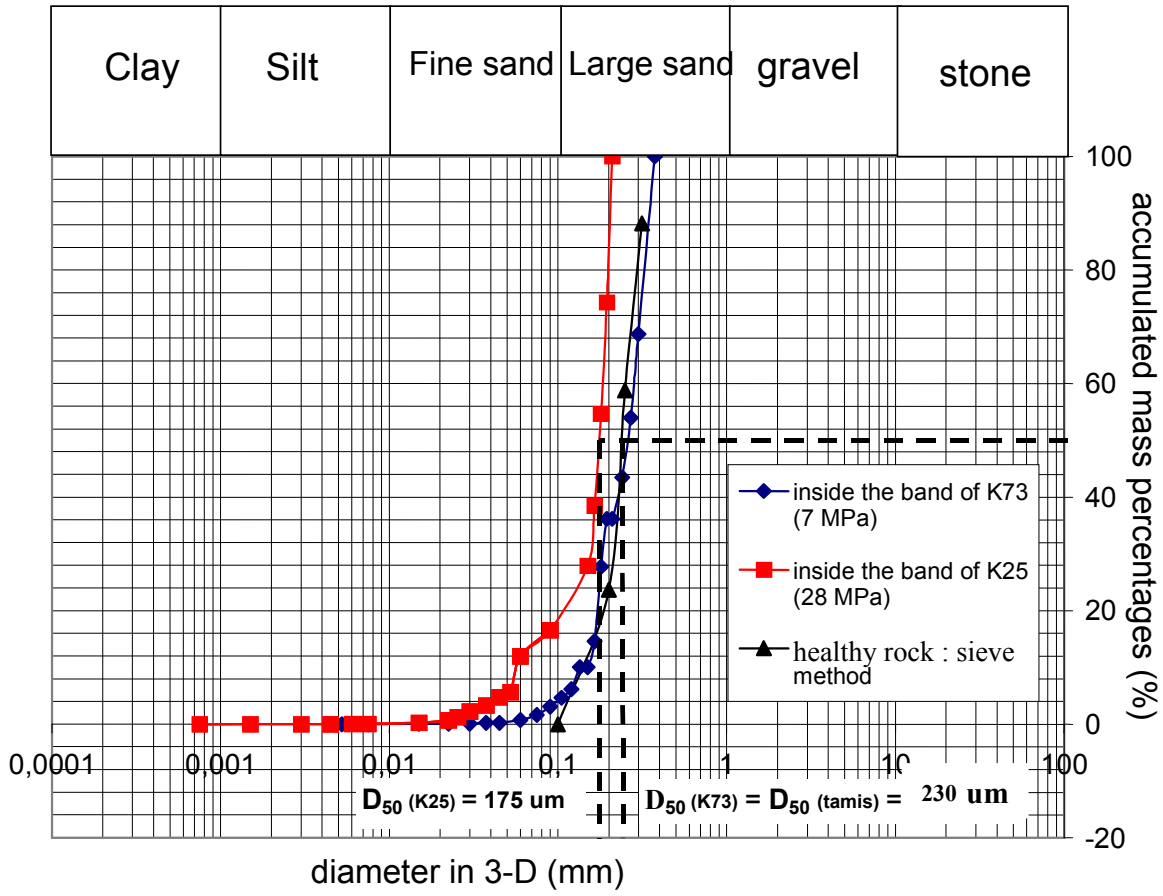
Clay
Silt
Fine sand
Large sand
gravel
stone
100
80
60
40
20
0
-20
accumulated mass percentages (%)
inside the band of K73 (7 MPa)
inside the band of K25 (28 MPa)
healthy rock : sieve method
0,0001
0,001
0,01
0,1
1
10
100
D50 (K25) = 175 um
D50 (K73) = D50 (tamis) = 230 um
diameter in 3-D (mm)

Figure 23

confinement pressure (MPa)	tests conditions	orientation of the shear band (°)	average value (°)
7	dry	68.5	65.5
7	dry	62.5	
14	dry	67	64.4
14	dry	62.3	
14	saturated	66.3	
14	saturated	62	
28	dry	61.5	60.4
28	saturated	62	
28	saturated	56.5	
42	dry	44.5	48.6
42	saturated	52.7	

Table 1

confining pressure (MPa)	tests conditions	shear band thickness (mm)	average value (mm)
7	dry	1.19	1.17
7	dry	1.16	
14	dry	0.7	0.8
14	saturated	0.7	
14	saturated	0.9	
14	saturated	1.1	
28	dry	0.64	0.66
28	dry	0.74	
28	saturated	0.59	
28	saturated	0.64	
28	saturated	0.7	
42	dry	0.57	0.53
42	dry	0.65	
42	dry	0.71	
42	saturated	0.43	

Table 2

Volumetric porosity (%)	Linear porosity (%)
5	5,02
6	6,15
21	21,3
28	27,8

Table 3